Sustained Ignition of an Undergraduate Hall Effect Thruster

IEPC-2024-150

Presented at the 38th International Electric Propulsion Conference, Toulouse, France
June 23-28, 2024

Albert Countryman*
Department of Physics, Brandeis University, 415 South Street, Waltham MA 02453

Braden Oh†, Avery Clowes‡, James Jagielski§, Lily Dao†, and Christopher Lee¶
Olin College of Engineering, Needham, MA, 02492

Mahderekal Regassa‖
Department of Physics, Wellesley College, 106 Central Street, Wellesley, MA 02481

In 2022, a team of undergraduate students conducted an independent study in which they designed, fabricated, and attempted to ignite a small, low-cost Hall effect thruster scaled from an SPT-100. In early 2023, the team was able to achieve stable ignition of the thruster during two rounds of testing, becoming the first undergraduate team to accomplish the feat. Spectrometer measurements were used to verify production of both krypton ions and argon ions. Operational parameters were determined (12.4 mN thrust at 628 W power) and compared to theoretical values predicted by Hall thruster scaling laws (13.0 mN thrust at 277 W power). However, the power efficiency was low at 0.20 as compared to 0.46 predicted. This paper also details the procedures used to achieve firing as a guide for future teams with limited experience operating Hall thrusters. This achievement further signals that Hall thruster development, fabrication and testing can serve as an educational vehicle for introducing the study of plasma and other advanced physics and engineering concepts to undergraduate students.

*Undergraduate, Physics, acountryman@brandeis.edu
†Undergraduate, Physics
‡Undergraduate, Mechanical Engineering
§Undergraduate, Electrical Engineering
¶Professor of Mechanical Engineering
‖Undergraduate, Physics

Copyright 2024 by the Electric Rocket Propulsion Society. All rights reserved.

Nomenclature

λ = ionization mean free path
v_n = neutral particle velocity
n_e = plasma electron number density
$\langle \sigma_i v_e \rangle$ = ionization reaction rate coefficient for species i
$\dot{m}_i$ = mass flow rate of ionized propellant
M = atomic mass of propellant
v_{ex} = final exhaust velocity of accelerated ions
A_c = area of thruster channel
p_i = particle utilization fraction
$\dot{m}_n$ = mass flow rate of neutral propellant
k_b = Boltzmann's constant
T_{room} = room temperature
θ = angle of propellant injection
L = length of ionization region
k_λ = coefficient used during calculation of ionization mean free path
P = thruster power generation
T = thrust
I_{sp} = specific impulse
η = thruster power efficiency
e = elementary charge
V_d = anode/ground voltage

Copyright 2024 by the Electric Rocket Propulsion Society. All rights reserved.

I. Introduction

A team of undergraduate students has previously constructed two Hall effect thrusters, a 19.5 mm permanent magnet thruster (Olin HET Mk I) [1] and a 50 mm electromagnet thruster (Olin HET Mk II) [2]. The Mk I thruster was tested in 2020, but was unable to sustain a stable plasma. The Mk II thruster was tested in 2022, but was unable to achieve ignition due to the limited electron generation of its cathode. Instead of a conventional plasma-source cathode, electrons were produced by short-circuiting a tungsten filament placed in close proximity to the thruster channel exit plane. For a detailed discussion of the design and initial testing of the Mk II, see [2]. Following that testing, the team obtained a barium oxide (BaO) hollow cathode (Plasma Controls LLC, Fort Collins, CO) which was able to provide sufficient current to achieve ignition during two rounds of testing. The first round of testing was in January 2023 at the MIT Space Propulsion Laboratory's AstroVac chamber, and the second round of testing was in April 2023 at the 10 m^3 vacuum tank at the Northeastern University Plasma Lab. This paper details the testing procedure used during the two rounds of trials, analysis of the spectroscopy data gathered during the second round of testing, characterization of thruster performance, a discussion of plasma instabilities observed during the first round of testing, and detailed instructions for the procedure used to ignite both the thruster and hollow cathode.

Shortly after publishing the 2022 paper detailing low-cost design methods for Hall effect thrusters, research groups at several other institutions began to publish work regarding undergraduate electric propulsion projects [3–5]. The success of these projects demonstrates the feasibility of the scope of such a project at an undergraduate level, and hence the necessity for a guide detailing low-cost design and testing methods to enable the further proliferation of such projects.

II. Testing Procedure and Experimental Setup

A. Experimental Setup

Testing of the Mk II was performed in two stages: first, achieving a continuous discharge, and second, increasing the magnetic field and discharge current to nominal operating conditions. The goal of testing was to characterize thruster performance by measuring the operational power, the thrust generated, and the exhaust velocity of accelerated ions. Challenges with direct thrust measurement occurred at both testing sites and are reported here for improving future instrumentation and to advise future student teams performing tests with a low instrumentation budget.

The vacuum-side experimental setup consisted of attaching the thruster to a vertical lever-arm thrust stand placed within the vacuum chamber, along with a circuit used for processing data for export to an air-side computer. A detailed diagram and description of the thrust stand used can be found in [2]. Power supplies for the four key power circuits (anode, cathode keeper, cathode heater, and electromagnets) were controlled via separate power supplies located outside the chamber. Real-time measurements of current and voltage were taken manually by operators. During the first round of testing, propellant flow to both the anode and cathode were controlled manually with needle valves. During the second round, flow was controlled by automated mass flow controllers. Continuous, steady firing of the device was confirmed by visual examination of plasma formation in the thruster channel during both rounds of testing and by spectrometer measurements during the second round of tests. A brief description of the procedure used to achieve firing is given below, but a detailed step-by-step and troubleshooting process for hollow cathode and thruster ignition can be found in Appendices A and B, respectively.

The ignition sequence is as follows: the hollow cathode is ignited, producing a current that is drawn into its keeper plate. Next, the thruster anode plate is set to draw current from the cathode. Neutral gas is flowed from the diffuser, set to collide with the electrons supplied by the cathode. Once the thruster channel plasma has ignited, the beam is confined by alternating increases of the electromagnet current and anode current. This prevents a sudden sharp decrease in anode current that could potentially extinguish the device. This process was used successfully to create steady plasma at multiple power levels at both testing sites. However, the specific test setups and instrumentation used varied by location.

Copyright 2024 by the Electric Rocket Propulsion Society. All rights reserved.

B. First Round of Testing

The first set of successful trials of the Mk II thruster were performed in the MIT Space Propulsion Laboratory's AstroVac chamber. The thrust stand and force sensor were configured in the same manner as in the initial round of testing reported in [2]. The thruster was hung from a pendulum arm held stationary by a piezoresistive force sensor configured as a Wheatstone bridge. The differential voltage across the bridge was carried to the outside of the chamber to an amplifier circuit, and the amplified signal was recorded by an Arduino Uno. Power supply data was collected manually.

Unfortunately, thrust data could not be collected during this testing due to excessive noise in the signal voltage. This noise was likely caused by the fact that relatively long, unshielded wires were used to carry the Wheatstone bridge voltage to the air-side amplifier circuit. This problem was compounded by the 10-bit resolution of the Arduino's analog-to-digital converter (ADC) which made it impossible to separate millinewton-scale thrust from signal noise.

The last notable problem with the testing at AstroVac was the issue of unevenness in plasma distribution, associated with the design and material selection of the gas diffuser. The original diffuser design possessed four helical tubes that injected propellant at an angle, with the intention of directing propellant velocity along the azimuth of the channel [2]. The lack of continuous rotational symmetry of the gas injection sites resulted in a lack of rotational symmetry of plasma density, as can be seen in Fig 1. During testing, the high-density regions of plasma within the channel would either remain stationary, or would coalesce into a single high density segment and revolve around the channel in the direction of $\vec{E} \times \vec{B}$. Upon examination of the state of the diffuser following operation, the stereolithographic resin (Somos PerFORM, Stratasys LLC, Eden Prairie, MN) that had been used to print the component had experienced extensive cracking and flaking. Exposure to high temperature during operation had widened the holes in the diffuser, likely worsening the rotational asymmetry of gas injection.

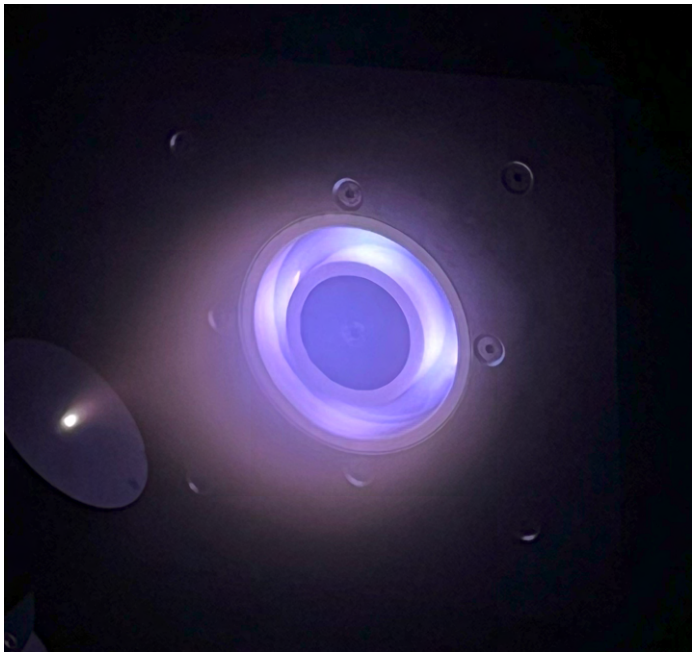

Figure 1: Krypton discharge generated by sustained ignition during first round of testing. Bright spots along thruster channel are located at gas injection sites

The successes of the first round of trials were achieving stable ignition for the first time and identifying the corresponding operating conditions (propellant flow rate, anode power, etc.). In addition, difficulties during testing highlighted thruster and instrumentation design changes to put in place in the following set of trials.

Copyright 2024 by the Electric Rocket Propulsion Society. All rights reserved.

C. Design Iterations

To perform in situ calibration of the force sensor, the thrust stand was augmented with a string-weight calibration rig similar to those presented in [6, 7]. In this scheme, a fishing line containing a series of small masses is hung at one end from a winding motor. The other end of the line is draped over a pulley to be directed perpendicular to the thrust stand pendulum arm and is affixed to the arm directly behind the thruster, as illustrated in Fig. 2. Raising and lowering the individual weights applies a known force to the pendulum, and the corresponding change in force signal is measured. This system thereby allows in situ force sensor calibration.

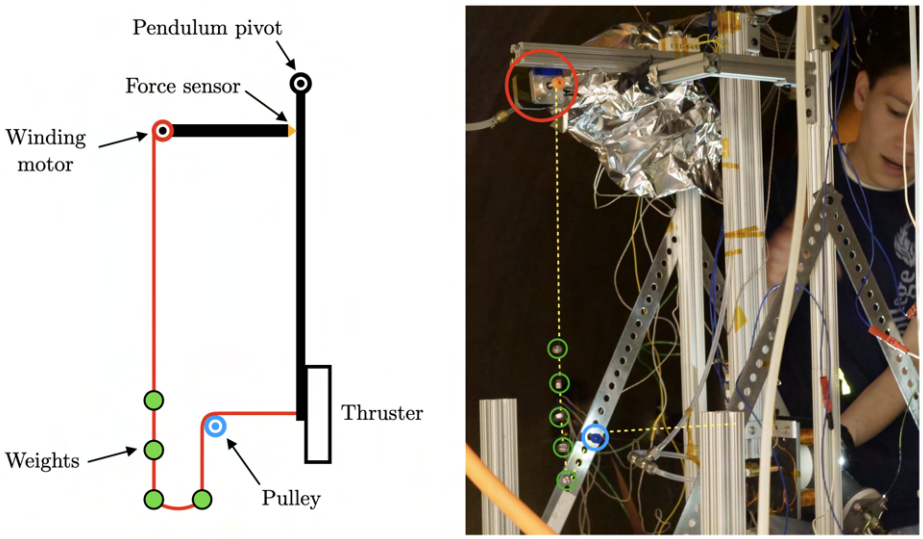

Figure 2: Diagram of the key components and relative geometries of the calibration rig (left) and a photograph of the system being installed in the test chamber (right), with winding rotor (red circle), weights (green circles), pulley (blue circle), and string (yellow dashes) highlighted

Two alterations were made to the thrust stand circuitry (see diagram in Fig. 3). For the first change, a higher voltage was applied across the Wheatstone bridge in order to increase the sensitivity of the sensor's force response. Accompanying this change, the signal amplification and measurement was moved to take place in-situ. A Raspberry Pi Pico (Raspberry Pi Foundation, Cambridge, England) was placed close to the Wheatstone bridge and signal amplifier to reduce the effect of electromagnetic interference on long signal lines. A Pico was used instead of an Arduino because of the significantly higher resolution of its ADC, at 16-bits instead of 10-bits. The Pico recorded the measurement signal and relayed data through the chamber wall over I2C lines. The I2C protocol enabled two-way communication through the chamber wall, also allowing the Pico to serve as the motor controller for the calibration motor. A schematic of the electrical system going into and out of the vacuum chamber can be found in Fig. 3.

The second design change was made to the thruster propellant diffuser. To produce a more even plasma distribution and to protect the diffuser from thermal damage, the design of the diffuser was altered in three ways: first, the number of dispenser tubes in the diffuser was increased from 4 to 70; second, the diameter of the dispenser tubes was reduced; and third, ribs were added to the outside face of the diffuser to reduce conductive heat transfer from the boron nitride channel walls. Diagrams of both versions of the diffuser are shown in Fig. 4. A nonprovisional patent for both designs was filed in May 2023.

D. Second Round of Testing

A second round of tests that was done at Northeastern University Plasma Research Laboratory allowed for measurement of the spectrum of radiation emitted by the plasma (which, indirectly, can also yield a measurement for the velocity of propellant ions departing the thruster channel). To measure this spectrum

Copyright 2024 by the Electric Rocket Propulsion Society. All rights reserved.

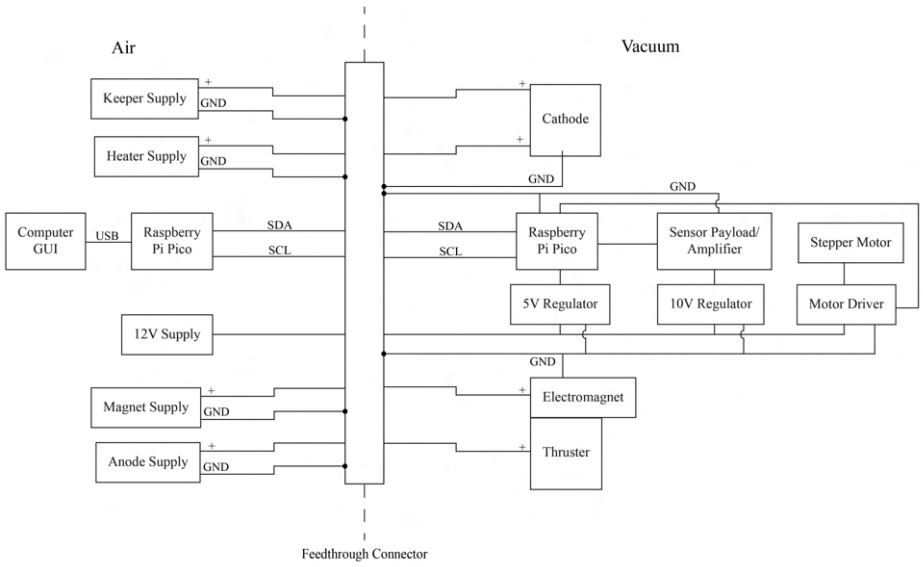

Figure 3: Electrical feedthrough diagram used to control thruster and receive experimental data.

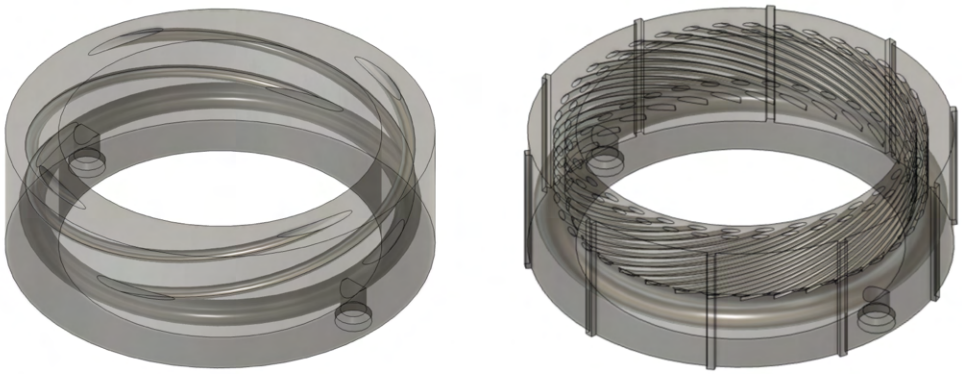

Figure 4: Diagrams of the initial (left) and final (right) iterations of the propellant diffuser

and the ion exhaust velocity, a spectrometer was aimed at the thrust plume and oriented perpendicular to the direction of the plume, enabling measurement of plume composition.

Unfortunately, communication issues with the in-situ Pico repeatedly occurred when vacuum was pulled, preventing thrust data from being collected. A solution to this issue would be to place the signal amplification circuitry inside the vacuum chamber and to carry an amplified measurement signal outside of the chamber on shielded lines. This architecture should serve to reduce the line-induced noise observed during testing at AstroVac and the risk of unexpected microelectronic failure in vacuum. However, a Pico will still be used to measure the signal on the air-side of the chamber, so as to utilize its low-cost 16-bit ADC.

Although thrust and ion velocity measurements were unable to be taken during this round of testing, successful measurement of the operational power and neutral propellant mass flow rate can be paired with an estimate of specific impulse to determine the performance of the device.

III. Results and Analysis

Thruster performance was characterized by the data collected during the second round of tests. This section discusses the results of the spectroscopy, the extrapolated performance of the thruster, along with plume

Copyright 2024 by the Electric Rocket Propulsion Society. All rights reserved.

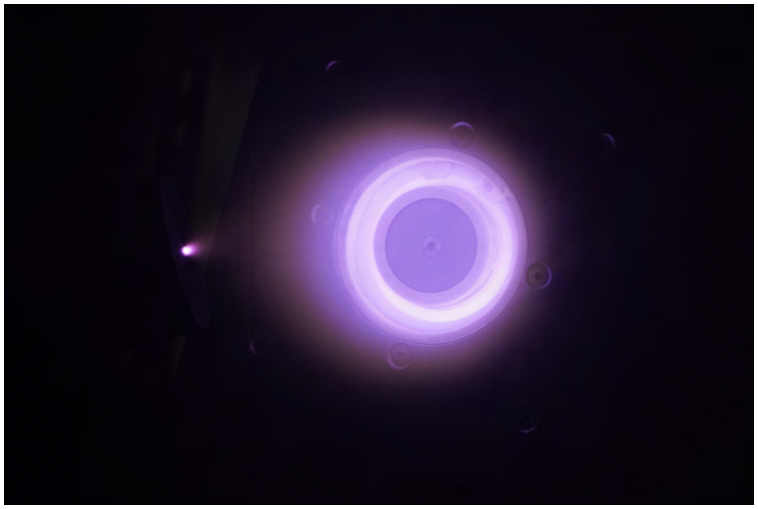

Figure 5: Krypton plasma generated during second round of testing. As a result of the more even distribution of neutral propellant, plasma distribution is even throughout the channel.

instabilities observed during the first round of tests. In this section "spectroscopy" refers to measurements of plume composition from the perpendicular spectrometer.

A. Spectroscopy

Plume composition measurements were made with the perpendicular spectrometer for both argon and krypton discharges. The emission spectra gathered by Adler et al. [8] for each are shown in Figs. 7 and 8, respectively.

During testing with both propellants, a discharge was initially struck without a magnetic field and the plume was visually observed while the magnetic field was increased. The color of the plume was used as a preliminary indicator for ion formation, as the plume distinctly shifted from pink/purple to blue as the magnetic field strength was increased. Numerous spectrometer measurements were attempted for argon at various magnetic field strengths, but the signal-to-noise ratio in the Ar+ emission band was often too weak to make a successful measurement. The spectrum shown in Fig. 7 was the only successful argon measurement made and confirmed that a low number of argon ions were indeed generated.

By contrast, the krypton emission spectrum was successfully measured at a variety of magnetic field strengths. Fig. 8 superimposes the results of discharges made at 0A and 0.7A of electromagnet current (corresponding to 0mT and 7mT of peak radial magnetic field strength, respectively). In this figure it is readily apparent that emissions in the Kr+ emission band dramatically increase at higher magnetic field levels, implying successful ion production.

In both spectra, emissions in the hydroxyl (OH) and cyanide (CN) radical emission bands are visible [9, 10] and a hydrogen alpha (H_α) emission [11] appears at high magnetic field strengths for krypton. These emissions are likely caused by particles from the propellant diffuser, which was made from Somos PerFORM and was directly exposed to the channel plasma. Although the chemical composition of PerFORM is not publicly available, the Material Safety Data Sheet for the fluid resin lists "epoxy" and "multifunctional acrylate" ingredients. From this, it is not unreasonable to assume that PerFORM contains hydrogen, carbon, oxygen, and nitrogen comprised molecules. By considering nylon, a generic synthetic molecule comprised of carbon (C), hydrogen (H), oxygen (O), the OH, CN, and H_α emissions can be explained as follows.

At high temperatures in inert environments, nylon undergoes pyrolysis, forming hydrogen cyanide (HCN) and releasing trapped water (H_2O) [12, 13]:

$$\text{Nylon} \Rightarrow HCN + H_2O. \tag{1}$$

When ionized, HCN and H_2O each dissociate, losing a hydrogen atom to become cyanide (CN) and hydroxyl

Copyright 2024 by the Electric Rocket Propulsion Society. All rights reserved.

Figure 6: Side view of krypton plasma generated during second round of testing at maximum electromagnet current of 0.85A. Presence of magnetic field causes the center of the discharge beam to cohere into a faint characteristic inverted-cone shape.

(OH) ions, respectively [14–16]:

$$HCN \Rightarrow H + CN \tag{2}$$

$$H_2O \Rightarrow H + OH. \tag{3}$$

Charges are left off of the molecules in the above expressions because it is not known which ions are formed in the thrust plume (electron bombardment can form the positive ions CN^+ and OH^+ [14, 15] while liquid solutions form the negative ions OH^- and CN^- [16]). Regardless of the ion species, the presence of OH, CN, and H-alpha emissions implies the presence of ionized diffuser particles in the thrust plume.

B. Mean Free Path

A quantity of interest for predicting thruster performance is the neutral particle ionization mean free path length. During the initial design process for the Mk II thruster this path length proved difficult to estimate. This calculation is revisited here in order to assist in estimating the ionization fraction of input propellant.

The plasma generated by the thruster occupies some length along the axis of the channel, referred to as the ionization region length, L. The ionization mean free path of a neutral particle, λ, represents the average distance that it will travel within the plasma before experiencing an ionizing collision. The fraction of incoming propellant that is ionized before leaving the channel, p_i, is a function solely of the ratio $\frac{L}{\lambda}$, described in Goebel and Katz Eq. 7.2-15 [17]. In order to receive the most thrust per input propellant, it is ideal to reach as close to 100% ionization as possible. As such, design of the thruster should be configured to minimize the length of the mean free path, which can be calculated using Eq. 7.2-14 in Goebel and Katz as

$$\lambda = \frac{v_n}{n_e \langle \sigma_i v_e \rangle} \tag{4}$$

which shows λ to be a function of the axial neutral particle velocity, v_n, the density of electrons in the channel, n_e, and an ionization reaction rate coefficient, $\langle \sigma_i v_e \rangle$. An estimate of n_e can be obtained by combining Eq. 7.3-55 (which assumes quasineutrality, that the density of positive ions in the plasma is equal to the density of electrons) and 2.3-7 in Goebel and Katz to yield,

$$n_e = \frac{\dot{m}_i}{M v_{ex} A_c} \tag{5}$$

Copyright 2024 by the Electric Rocket Propulsion Society. All rights reserved.

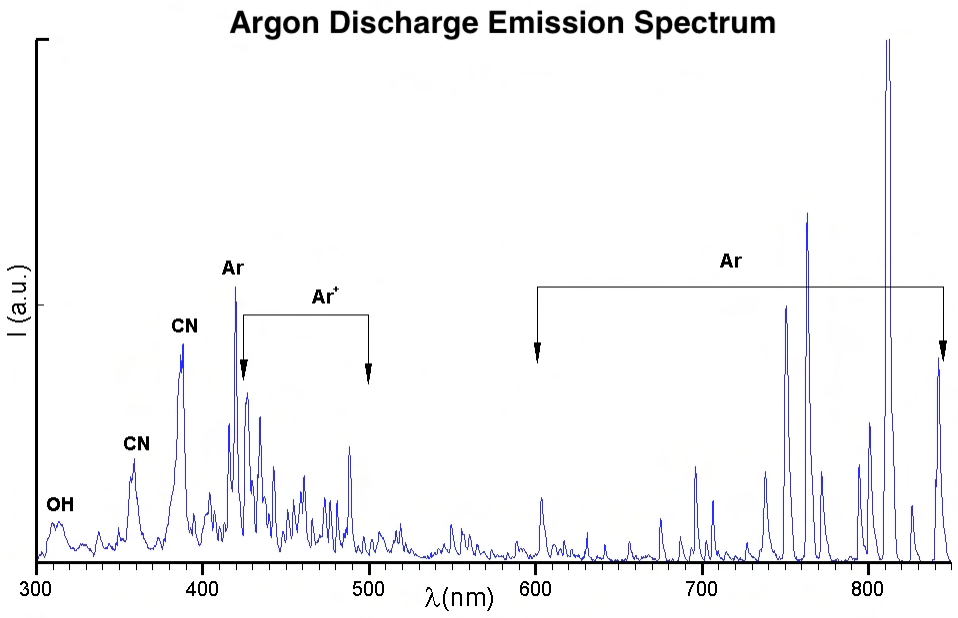

Figure 7: Plume emission spectrum for an argon discharge (y-axis intensity is measured in arbitrary units). The low intensity of Ar+ emission indicates that low quantities of Ar+ ions are being created.

where M is the atomic mass of propellant, A_c is the area of the thruster channel, $\dot{m}_i$ is the mass flow rate of ions out of the channel, and v_{ex} is the exhaust velocity of expelled ions. Given that $p_i \equiv \frac{\dot{m}_i}{\dot{m}_n}$ (where $\dot{m}_n$ is the mass flow rate of neutral particles into the channel), this can be expressed as

$$n_e = \frac{p_i \dot{m}_n}{M v_{ex} A_c}. \tag{6}$$

Due to the low density of propellant within the diffuser and vacuum chamber the propellant behaves as a molecular gas, and not a continuous fluid [18]. As such, fluid dynamical equations cannot accurately describe quantities such as the velocity of the neutral propellant; instead, the gas can be considered as a set of ballistic particles described by the Boltzmann equation. Given that the particles are confined to travel in 1D across the length of the tubing, we can expect the distribution of velocities to follow a 1D Maxwell-Boltzmann probability distribution function. The average speed predicted by this distribution is

$$v_n = \sqrt{\frac{2 k_b T_{\text{room}}}{\pi M}} \tag{7}$$

where k_b is the Boltzmann constant and T_{room} is the temperature of the gas. Finally, the quantity $\langle \sigma_i v_e \rangle$ is computed empirically by measuring the cross section of the collision at varying electron energies. A process of how to compute this quantity can be found in [17]. For krypton ions with an average temperature of 30eV, this value is 6.65×10^{-14} m^3/s. A unified expression for the mean free path is therefore

$$\lambda = \sqrt{\frac{2 M k_b T_{\text{room}}}{\pi}} \frac{v_{ex} A_c}{\dot{m}_n p_i \langle \sigma_i v_e \rangle}. \tag{8}$$

The above equation applies, in general, to an arbitrary thruster using a propellant injection system which directs gas velocity along the axis of the channel. The term v_n, however, represents the component of neutral velocity directed toward the cloud of electrons. For a thruster with a non-axial injection system such as the Mk II, an angular correction factor must be introduced to Eq. 7, corresponding to the angle θ at which gas is introduced to the channel:

Copyright 2024 by the Electric Rocket Propulsion Society. All rights reserved.

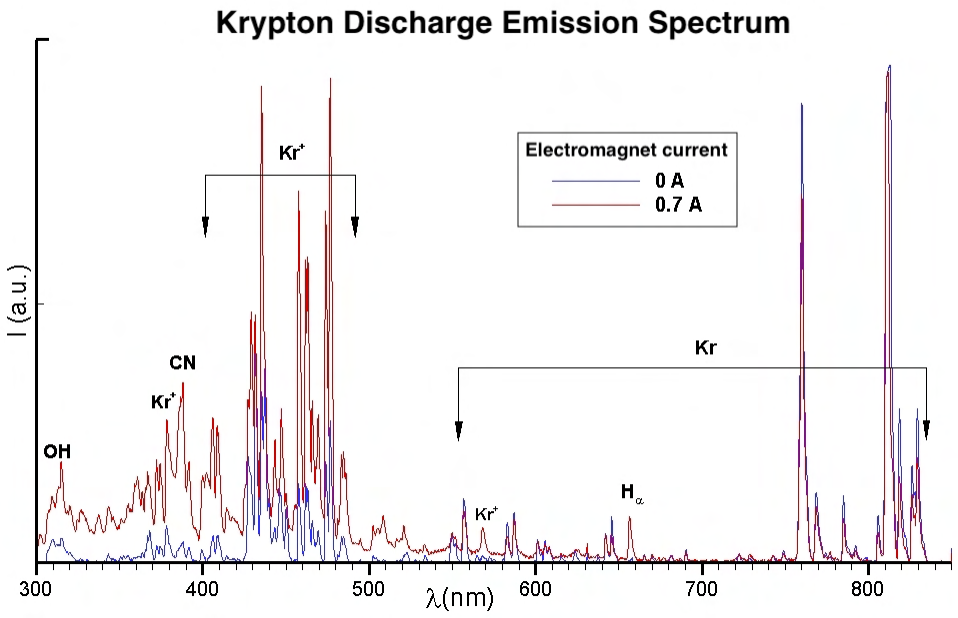

Figure 8: Plume emission spectrum for krypton discharges at electromagnet currents of 0A and 0.7A (y-axis intensity is measured in arbitrary units). The high intensity of Kr+ emissions at the higher magnetic field indicates successful production of Kr+ ions as a result of the channel Hall current.

$$\lambda = \sqrt{\frac{2Mk_bT_{\text{room}}}{\pi}} \frac{v_{ex}A_c}{\dot{m}_n p_i \langle \sigma_i v_e \rangle} \sin(\theta). \tag{9}$$

The above equation provides an expression for λ that depends on p_i, and Eq. 7.2-15 in Goebel and Katz provides an expression for p_i that depends on λ,

$$p_i = 1 - \exp\left(-\frac{L}{\lambda}\right). \tag{10}$$

Taken together, Eq. 9 and 10 can be used to solve for the two unknowns, λ and p_i. Substituting Eq. 10 into Eq. 9 yields,

$$\lambda = \sqrt{\frac{2Mk_bT_{\text{room}}}{\pi}} \frac{v_{ex}A_c}{\dot{m}_n \langle \sigma_i v_e \rangle \sin(\theta)} \frac{1}{1 - \exp\left(-\frac{L}{\lambda}\right)} \tag{11}$$

$$\lambda \equiv \frac{k_\lambda}{1 - \exp\left(-\frac{L}{\lambda}\right)}. \tag{12}$$

Eq. 12 has no closed-form solution, but can be numerically evaluated for given values of k_λ and L. The length of the ionization region is difficult to estimate, so here it is assumed that the plasma generated within the channel occupies a length on the scale close to that of the channel itself (10^{-2}m). For the operating conditions of the OHET Mk II (see Sec. C for discussion on estimating exhaust velocity), this results in a mean free path length of $\lambda = 8$ mm and a particle ionization rate of $p_i = 71\%$.

C. Thruster Performance

An evaluation of the performance of a thruster generally considers three main quantities which describe the fuel and energy efficiency of the thruster: the power used (P), the thrust generated (T), and the specific impulse (I_{sp}).

Copyright 2024 by the Electric Rocket Propulsion Society. All rights reserved.

Power efficiency is calculated as the ratio between the power required to run the thruster and the power of the ion beam (the time-rate of change of outgoing kinetic energy of the expelled fuel). The ratio between these two quantities, η, represents the energetic losses incurred during thruster operation.

The structure of this section is as follows: first, scaling laws for η and I_{sp} are derived based on reported scaling laws for P and T. Next, these scaling relations are applied to the design of the OHET Mk II in order to determine how its performance parameters compare to those of standard Hall thrusters with similar physical dimensions, operational mass flow rate, discharge voltage, and ionization fraction p_i.

An HET discharge can be analyzed as a circuit. Plasma in the channel is a resistive medium transmitting current from the anode to the cathode (*i.e.*, electrons use the plasma as a pathway from the cathode to the anode and positive ions are accelerated away from the anode). As such, the power of the thruster depends on the voltage and current being supplied to the anode and cathode ($P_{circuit} = I_d V_d$, where I_d represents the anode current and V_d represent the voltage between the anode and ground). By measuring these quantities (along with $\dot{m}_i$ and v_{ex}), it is possible to calculate the device's power efficiency η by dividing the rate of change of ion beam kinetic energy by the power taken to operate the circuit as

$$\eta = \frac{\dot{m}_i v_{ex}^2}{2 I_d V_d}. \tag{13}$$

Using the above metrics to describe thruster operation, the measured performance of the thruster can be compared to scaling-law predictions described in [19]. The design of the thruster is based on a half-scale SPT-100, using the scaling relations reported by Goebel and Katz [17]. Since the release of that book, however, a more comprehensive set of scaling laws has been reported by Lee *et al.* [19]. Performance predictions made by scaling the SPT-100 according to Lee *et al.* are used here as the benchmark against the Mk II thruster. Where the Goebel and Katz scaling relations depend only on choice of thruster channel radius, the Lee *et al.* scaling relations depend on the thruster channel width w, channel radius R, and discharge voltage V_d. Although these laws describe the scaling of T, P, w, $\dot{m}_n$ (and not I_{sp} or η), they can be combined to produce a scaling law for I_{sp} and η by rearranging the laws for P and T. Beginning with Eq. 9 from Lee *et al.*,

$$P \approx \frac{e p_i}{M} \dot{m}_n V_d \tag{14}$$

where e is the elementary charge. Because the two flow rates are proportional to one another ($\dot{m}_i = p_i \dot{m}_n$), they can be interchanged for the purposes of scaling. Although Lee *et al.* prescribes a scaling law for mass flow rate that would allow this expression to be put in terms of thruster radius R, this law was not used to select a mass flow rate during testing and thus the final scaling law for P is as follows:

$$P \propto \frac{p_i \dot{m}_n V_d}{M}. \tag{15}$$

Note that while M is normally constant and can be removed from the scaling expression, it must be left intact if the type of propellant used is changed between thrusters. Using Eq. 2 from [2], this can be expressed as

$$\frac{p_i \dot{m}_n v_{ex}^2}{\eta} \propto \frac{\dot{m}_i V_d}{M}. \tag{16}$$

Using the definition of thrust T from Eq. 3 in [2] this can be re-written as

$$\frac{T^2}{p_i \dot{m}_n \eta} \propto \frac{p_i \dot{m}_n V_d}{M}. \tag{17}$$

Combining Eq. 15-18 from Lee *et al.*, the thrust T will scale as,

$$T \propto p_i \dot{m}_n \sqrt{\frac{V_d}{M}}. \tag{18}$$

Substituting this into Eq. 17 yields,

$$\frac{p_i \dot{m}_n V_d}{M \eta} \propto \frac{p_i \dot{m}_n V_d}{M} \tag{19}$$

Copyright 2024 by the Electric Rocket Propulsion Society. All rights reserved.

$$\Rightarrow \frac{1}{\eta} \propto 1. \tag{20}$$

This result implies that as the thruster is scaled in the sub-kilowatt regime described by Lee *et al.*, power efficiency can be treated as a constant. Now, combining Eq. 1-3 from [2], I_{sp} can be expressed as

$$I_{sp} = \frac{2\eta P}{gT} \Rightarrow I_{sp} \propto \frac{P}{T}. \tag{21}$$

Using Eq. 15 and Eq. 18,

$$I_{sp} \propto \frac{p_i \dot{m}_n V_d}{M} \cdot \frac{1}{p_i \dot{m}_n \sqrt{\frac{V_d}{M}}} = \sqrt{\frac{V_d}{M}}. \tag{22}$$

Thus, it can be expected that scaling the specific impulse depends only on the anode discharge voltage and the mass of propellant chosen.

The Mk II thruster has a channel width and radius half that of the SPT-100 and a discharge voltage approximately equal to that of the SPT-100 [2], and used a different mass flow rate and propellant. Additionally, the SPT-100 ionizes nearly 100% of input propellant, while the OHET Mk II operates with an ionization fraction of approximately 71%. Using these alterations with the scaling laws in Lee *et al.*, the predicted operating parameters of Mk II thruster are listed in Table 1 alongside the nominal operational parameters for the SPT-100 also reported by Lee *et al.*

Although the original scaled parameters predicted for the OHET Mk II were determined based on scaling the channel radius, scaling law dependence on thruster radius sources from utilizing a mass flow rate that scales proportional to wR [19] (ensuring that as the thruster is scaled, the density of neutral particles flowing into the channel is left unchanged). Because the Mk II did not operate using a mass flow rate which was scaled proportional to wR, computation of scaled values depends on the ratio between the mass flow rates used by the OHET and the SPT-100 (as opposed to the ratio between thruster radii).

Table 1: Comparison of OHET Mk II operational values to SPT-100 and Scaling Law predictions. Source: Lee *et al.* [19]

	SPT-100	OHET Mk II Measurements	Scaling Predictions
Discharge Voltage (V)	300	316	298
Channel Width (mm)	15	7.5	7.5
Channel Outer Radius (mm)	50	25	25
Mass flow rate (mg/s)	5.14	0.90	0.90 [a]
Power (W)	1350	628	277
Thrust (mN)	81.6	12.4 [c]	13.0
Specific Impulse (s)	1540		1978 [b]
Power Efficiency η	0.46	0.20 [c]	0.46 [b]
Ionization Fraction	100%	71% [c]	71% [c]

[a] This value does not correspond to the scaled mass flow rate described in Lee *et al.*
[b] This value was computed using a scaling law derived in section C.
[c] This value was computed using the scaled value for I_{sp}.

As can be seen in Table 1, the OHET Mk II exceeded scaling law expectations with respect to operational power and produced an amount of thrust close to what is predicted by scaling laws. However, power efficiency of the Mk II did not measure up to the scaling law prediction determined for η.

D. Magnetic Field Strength

Aside from a scaling law-based analysis of thruster performance, another operational parameter to examine is the strength of the magnetic field that was able to be present along with a stable plasma. The magnetic

Copyright 2024 by the Electric Rocket Propulsion Society. All rights reserved.

field is necessary to confine the plasma within the channel, which is responsible for two important processes. Firstly, beam confinement directs ions along the axis of the channel so that the velocity of expelled particles contributes maximum momentum of the craft. Secondly, the presence of a strong magnetic field traps more electrons within the ionization region of the channel, increasing the density of electrons present and hence raising the ionization fraction of the propellant. The thruster magnetic circuit was designed to sustain a nominal magnetic field strength of 30 mT at the channel exit plane, a value similar in magnitude to thrusters designed by Baird [20] and Warner [21]. Such a field strength was found to be achieved at a current of 3 A running through the electromagnet circuits. During the operation of the thruster, however, a stable plasma was never able to be maintained at an electromagnet current higher than 0.85 A. Given that the thruster plume would extinguish itself after exceeding this value, it is theorized that this occurs as a result of the additional impedance introduced into the thruster circuit by a strong magnetic field. Given that the strength of each of the superimposed magnetic fields change roughly linearly with input current (discounting nonlinearities in the magnetization of ferromagnetic components), this would correspond to a peak magnetic field strength of approximately 8.5 mT, assuming approximately linear magnetization. Improving the device's efficiency and delivered thrust requires a design that is able to accommodate the presence of a stronger magnetic field.

E. Thruster Spoke Modes

It is hypothesized that the observed rotational behavior of the plasma created during the first round of testing was an instance of the well-documented "spoke mode" instability common to Hall thrusters [22]. During testing, an $m = 1$ spoke mode was visually observed rotating around the Mk II channel at low magnetic field strengths. A video recording of the instability was processed using the OpenCV video stabilization and SciPy FFT libraries. A wave frequency of 1.65 Hz was determined at a magnet current strength of 0.1 A (corresponding to a peak magnetic field strength of approximately 1 mT, assuming approximately linear magnetization). A series of frames from the recorded video is shown in Fig. 9. As the magnetic field strength was increased, the rate of rotation was observed to increase in frequency.

Figure 9: Four frames from a video recording of the spoke instability. At the time of recording, a wave frequency of 1.65 Hz was measured.

After the redesigned diffuser was incorporated into the thruster, a distinct spoke mode instability could no longer be observed. The fact that no other operational parameters had been altered between the two sets of trials other than the distribution of injected gas implies that the low-frequency instability observed during the first round of trials was caused by the highly uneven distribution of propellant in the channel.

IV. Next Steps & Conclusion

The OHET Mk II is the first ion thruster built by a fully-undergraduate student team that has achieved steady-state operation. During two rounds of testing, the thruster demonstrated stable operation above 600 W at an estimated power efficiency of 19.7% and predicted fuel utilization of 71%. A discharge was achieved with both argon and krypton propellant and spectroscopy was used to confirm the presence of Kr+ ions in the discharge plume. Additionally, a low-frequency spoke instability was visually observed at low magnetic field strengths. However, the discharge was observed to spontaneously extinguish as the magnetic field was increased towards the expected operational value.

Copyright 2024 by the Electric Rocket Propulsion Society. All rights reserved.

Beyond this initial demonstration, further work will be conducted in two primary areas: further measurement and characterization of the performance of the thruster and a redesign of the device to improve performance and incorporate design elements of contemporary Hall thrusters. Development of a heaterless cathode is also underway.

To increase the performance of future OHET thrusters, operation at higher magnetic field strengths must be achieved. Future design work (following greater characterization of the Mk II) will focus on the magnetic field geometry. Designing the magnetic field so that the field vanishes at the anode plate has been linked [17] to higher thruster performance. Additionally, some degree of magnetic shielding will be incorporated into future designs. Magnetic shielding is an effect caused by specially shaped magnetic field geometry which directs energetic ions away from channel walls in order to reduce erosion and extend the lifetime of the thruster [23]. New materials and methods for manufacturing the device's channel and gas diffuser will be investigated given the successful use of a 3D printed diffuser during Mk II testing. Although 3D printed channel and diffuser components will result in short thruster lifetimes, benefits of rapid, low-cost iteration through thruster component designs and magnetic field geometries are anticipated.

The successful operation of this 600W, steady-state Hall thruster demonstrates that electric propulsion and introductory plasma physics can feasibly be incorporated into an undergraduate education. This testing marks the culmination of a multi-year, self-directed educational process that has incorporated fundamental and applied physics, engineering design and manufacturing principles, and the practices of instrumentation and experimentation. The development of the Mk I thruster yielded a curriculum for an undergraduate independent study of Hall thruster principles [1], while development of the Mk II yielded a design process and exploration of Hall thruster physics [2]. This article documents the testing process and contains sample operational procedures for teams new to Hall thruster testing (see Appendices A and B). Taken together, this work may serve as a road map for future teams of students and educators seeking to access the exciting field of electric propulsion for the first time.

Acknowledgments

The authors thank Prof. John Williams and Seth Thompson for donating the hollow cathode used in these experiments and for providing invaluable guidance in creating the cathode and ignition procedures reported in this paper. The authors also thank Prof. Paulo Lozano and Matthew Corrado for donating their time and laboratory resources to allow testing at AstroVac. The authors also thank Prof. Oleg Batishchev, H. Adler, N. Hall and D. Wasserman for providing access to their vacuum facility, high-purity propellants, assistance with setting up and running the OHET Mk II, and for collecting and analyzing spectroscopic data. The authors also thank Dr. Dan Goebel for the loan of another plasma-source cathode and for providing extensive guidance throughout the entire project. The authors also thank Dr. Rebecca Christianson for providing invaluable advice and expertise that allowed the team to gain greater understanding of the physical principles involved in the operation of the thruster. Finally, the authors thank Pauline Petersen, Mihir Vemuri, and Sohum Kothavade for assistance setting up equipment and collecting data during the second round of testing.

This work was supported by funding from the Draper Laboratory Undergraduate Senior Capstone Project program, from the Babson College Weissman Foundry Fellowship program, and from the Massachusetts Space Grant Consortium.

Copyright 2024 by the Electric Rocket Propulsion Society. All rights reserved.

Appendix A Sample Cathode Ignition Procedure

Hollow cathodes create a plasma in a three step process: first, a thermionic material is heated to temperatures that allow emission of low-energy electrons; second, a high-voltage keeper is used to accelerate the electrons to high kinetic energy levels; and third, these electrons bombard a propellant gas to generate a plasma. This plasma forms a low-resistance bridge that allows electrons to flow from the emitter to the Hall thruster channel.

Barium oxide (BaO) and lanthanum hexaboride (LaB_6) are the most common emitter materials used in modern hollow cathodes. BaO has more flight heritage and a lower work function than LaB_6, so it can ignite a plasma at lower heater temperatures. However, it is more susceptible to "poisoning," a process in which the emitter reacts with oxygen or water to form a high-work function surface that prevents emission from occurring. Careful steps must be taken during cathode startup to avoid poisoning a BaO cathode. An example setup and operating procedure for a 1/4" BaO hollow cathode is given below. This procedure may generally be followed for igniting a LaB_6 hollow cathode as well. However, ignition temperatures may be higher and the gradual warm-up period may be skipped (as LaB_6 is resistant to poisoning).

Important note and disclaimer: A hollow cathode will have an experimentally determined heater power at which ignition can nominally occur. This power is determined by the thermal transport properties of the device. Furthermore, the resistance of a heater filament will increase with temperature, meaning current has a nonlinear relationship to heater power. As such, the heating parameters listed below are reported as *suggested percentages of the ignition current assuming a corresponding rise in filament resistance.* These percentages may not work for all cathodes!

First-time determination of ignition power:

To determine the ignition power for a cathode that has not been lit before, an iterative experimental process will need to be followed. Prior to beginning testing, the authors recommend performing a thermal simulation of the cathode with a tool such as COMSOL using the following boundary conditions:

- Constant power input at the heater surfaces.
- Radiation into an environment at room temperature (e.g. 293 K).
- Multi-layer insulated surfaces (i.e. wrapped in molybdenum foil) may be simulated by reducing the emissivity of the wrapped surface by 2^{-n}, where n is the number of layers.
- Fixed ambient temperature at the cathode fixture (i.e. the surface at which the cathode is attached to a mounting structure, chamber wall, heat sink, etc.).

With these boundary conditions, performing a sweep of heater input powers will yield a corresponding temperature at the emitter surface. The power for which the emitter reaches 1100°C can serve as the initial starting point for ignition testing. In general, these models under-predict the necessary heater power (i.e. in reality, thermal losses are higher), so when obtaining power supplies, margins of 30-50% are recommended. During live testing, the heater power should be incrementally stepped up from the simulated value until ignition is achieved. If increasing heater power alone fails to achieve ignition, increasing gas flow and keeper voltage (in that order) are additional variables to tune.

General cathode properties and power supplies:

- Keeper supply: 300V/1.5A DC
- Heater supply: 30V/10A DC
- 1/4" BaO emitter hollow cathode, orificed tube
- Likely ignition conditions:
  - 3-7 sccm Kr or 10-20 sccm Ar gas flow
  - 300V keeper voltage
  - Emitter temperature > 1100°C

Prior to pulling vacuum:

- Set keeper power supply current limit to 1A (or other desired current).

Copyright 2024 by the Electric Rocket Propulsion Society. All rights reserved.

- Verify keeper connection by applying a low voltage (e.g. 10-30V) and measure the voltage directly using a multimeter.
- Verify heater connection by measuring the resistance across the heater lines. A thin-filament heater will generally have a resistance of 0.5-2Ω[a].

Pull vacuum and pressurize gas lines:

- Upon pulling vacuum, open all valves and flow controllers on the propellant line all the way back to the bottle valve (but leave the bottle closed). Allow the air to *completely* bleed out of the propellant lines.
- Verify that an ultimate vacuum of 10^{-4} Torr or lower is achieved. Higher pressures could indicate leaks or material outgassing and risk poisoning the emitter.
- Close the flow controller or flow control valve (this may be an electronic controller or a manual needle valve) and close the bottle regulator valve (this is usually done by completely loosening the regulator knob).
- Open the propellant (Ar, Kr, Xe) bottle valve. The upstream regulator gauge should read high pressure and the downstream should still read closed.
- Slowly open the bottle regulator, pressuring the line to a nominal pressure for the flow controller (10-15 PSI is a safe set point for an Alicat M-100SCCM-D-I/5M).
- Open the flow control valve (or electronically command the flow controller) to 5 sccm gas flow and let run for 5-10 mins to make certain the lines are purged of oxygen.

Warm the cathode:

- Gradually warm the cathode to prevent thermal shock and to allow trapped water and other volatiles to outgas. The heating schedule followed by the authors is reported in Table 2.

Current [%]	30%	46%	62%	77%	85%	92%	100%
Time [mins]	30	30	5	5	5	5	5

Table 2: Example heating schedule for a 1/4" BaO hollow cathode. Current level is reported as a percent of nominal ignition temperature, *not* maximum heater temperature.

Ignite the cathode:

- To trigger ignition, rapidly increase the voltage on the keeper power supply towards 300V. Upon ignition, the keeper current will rail at the current limit and the discharge voltage will likely fall to the 10-40V range. The authors observed ignition near 160-180V for krypton and 200-250V for argon. A white/blue plasma discharge will emanate from the cathode.
- Upon ignition, **immediately reduce the heater current** to a maintenance power of 30% power or less. The amount of heater power necessary to sustain ignition decreases with current drawn from the cathode (as increased current increases ion bombardment of the emitter). Continuing to supply high current during operation will catastrophically damage the heater.
- Reduce the propellant flow if desired.

Cooling the cathode:

- Shut off the heater and keeper power supplies.

[a]Alternatively, current may be run through the heater to verify resistance (e.g. 1V→1A), but this must be done *extremely briefly*, as heating the filament in atmosphere can destroy it.

Copyright 2024 by the Electric Rocket Propulsion Society. All rights reserved.

- Set the propellant flow to 5 sccm and allow the cathode to cool for a minimum of 30 minutes (1-2 hrs is advisable) in high vacuum. **Warning:** exposing a hot cathode to oxygen-tainted pressures above 10^{-4} Torr could poison the emitter!
- Close the propellant bottle valve completely and leave the regulator and flow valves open to allow the lines to bleed (this avoids a pressurized line hazard).
- Shut down the vacuum pumps and vent the chamber.

Troubleshooting:

- If the plasma goes out after a few minutes of operation, it is likely that the emitter cooled below emission temperature. During normal operation, ions in the plasma bombard the surface of the emitter and keep it hot, but the thermal properties of a particular cathode may require additional heat to maintain emission temperature.
  - Repeat the ignition process, holding each temperature step for five minutes (the 30 minute wait periods are only needed for initial outgassing).
  - Upon successful ignition, reduce the heater current to a maintenance power 8% higher than was previously reduced to.
  - If the cathode goes out again, repeat this process until a stable maintenance power is found.
  - **Warning:** emitter heating due to ion bombardment is proportional to the amount of current being drawn from the plasma. For a 1A keeper and 1A thruster discharge, a total of 2A of ion current is striking the emitter. If greater currents are drawn from the plasma, it is advisable to reduce the maintenance power to avoid damaging the heater filament.
- If the cathode does not ignite at all for keeper voltages $\leq$ 300V, increases can be made to heater current, keeper voltage, and flow rate.
  - Begin by increasing heater current by a small amount and attempting ignition after five minutes. This may be repeated until nearing the maximum filament temperature.
  - Higher flow rates are particularly necessary for argon, which is more difficult to ionize than krypton and xenon. If ignition cannot be achieved at 300V with argon, switching propellants is advisable.
  - Increasing the keeper voltage should be the last step taken, as 300V should be enough to ignite noble gas propellants.
- If high heating currents and/or keeper voltages above 300V are necessary for ignition, this may indicate poisoning of the emitter (whose work function increases with oxidation).
  - Additional radiation shielding (generally molybdenum or tantalum foil) may be added to reduce radiative losses from the heater. Score or texture the surface of the foil prior to wrapping it around the cathode tube to reduce conductive losses through the foil. Also ensure that the foil does not contact the heater lead or keeper to prevent a short circuit.
  - If ignition is still not possible at high currents and voltages with extra shielding, the BaO may be critically poisoned and may need to be replaced.
- An abnormally high or low heater current flow may indicate a problem with the heater filament. Thin-filament heaters generally have 0.5-2 Ω of resistance at room temperature (though this resistance will change as filament heats up)
  - A continuity check may be used to confirm that there is a closed path through the filament to ground; $< 2\Omega$ of resistance should be low enough to register as continuous. If the continuity check fails, it is likely that the heater filament has broken.

Copyright 2024 by the Electric Rocket Propulsion Society. All rights reserved.

Appendix B Sample Thruster Ignition Procedure

When performing initial characterization of a thruster, the parameters for a stable discharge may be unknown. The following procedure outlines the process used by the authors to first determine a set of stable discharge parameters and then identify a set of nominal operating parameters for their Hall thruster.

An initial attempt to ignite a Hall thruster will occur in two stages: first, ignite a glow discharge, then achieve ionization via a Hall current. A glow discharge is relatively easy to strike, but contains few ions and is conceptually similar to the discharge in a fluorescent lightbulb. Most of the light generated comes from excited electrons and krypton and argon glow discharges have a distinct pink hue. On the other hand, a glow discharge indicates that a bridge has successfully formed between the cathode and anode, so it is a critical first step to confirming the cathode-thruster circuit. Glow discharges tend to be struck most easily without a magnetic field; by trapping electrons, a magnetic field effectively increases the impedance of the circuit and may prevent enough electrons from reaching the anode to strike a glow discharge.

Once a glow discharge is initiated, the magnetic field can gradually be turned up. As the magnetic field increases, electron trapping occurs and a Hall current forms in the channel. This Hall current performs propellant ionization and transitions the glow discharge into a high-ion plasma capable of generating thrust. The authors found this transition difficult to achieve.

Authors' power supplies and thruster properties:

- Anode: 300 V/2 A DC
- Magnet: 30 V/10 A DC
- Designed discharge power: 300 V/1 A (300 W)
- Designed magnet current: 3 A (30 mT peak strength)
- Designed flow rate: 20 sccm krypton

Before pulling vacuum:

- Select anode-cathode grounding scheme. The authors recommend connecting both the anode power supply reference and cathode emitter to earth ground for ease of implementation. For more "flight-like" behavior, it may be desired to "float" the cathode ground by directly connecting the cathode emitter to the anode power supply reference. The voltage on the cathode is thereby free to "float" relative to earth ground. The magnitude of the floating voltage may provide insight into how effectively thrust plume neutralization is occurring.
- Verify anode connection by applying a low voltage (e.g. 10-30 V) and measure the voltage on the anode directly with a multimeter.
- Verify electromagnet connection by continuity checking and/or by comparing the resistance of the electromagnet circuit within the thruster to the resistance across the electromagnet circuit leads outside the vacuum chamber.

Initiate glow discharge:

- Ignite hollow cathode.
- Begin thruster propellant flow.
- Turn on the thruster voltage (leaving magnet current off). A discharge should visibly ignite and the anode power supply will rail to its current limit at a relatively low voltage.
  - If a glow discharge is not seen, gradually increase propellant flow and/or anode voltage.
  - If a glow discharge is still not seen, it is likely that a problem in the circuit is preventing high voltage from making it to the thruster anode. Verify that the power supply connections outside and inside the chamber are correct.
  - The authors struck glow discharges easily with both argon and krypton propellants. The striking voltage of 300 V fell to near 50 V at 1 A of discharge current.

Copyright 2024 by the Electric Rocket Propulsion Society. All rights reserved.

Initiate Hall current:

- Very slowly, introduce a low magnet current (e.g. < 0.25 A). The anode voltage should rise. This corresponds to an increase in effective circuit resistance due to electron trapping.
- If the thrust plume disappears immediately upon introduction of the magnetic field, shut off the magnet current, allow the glow discharge to reappear, and then:
  - Increase the propellant flow rate. Attempt to reintroduce the magnetic field. Repeat until a stable discharge is reached.
  - If a significant increase to flow rate (e.g. 10-20 sccm) does not achieve a stable discharge, gradually reduce the flow rate while attempting to reintroduce the magnetic field. Repeat until a stable discharge is reached.
  - If adjustments to flow rate are not successful, introduce a slight increase to the anode current draw (e.g. 0.1 A at a time) while adjusting the flow rates in either direction.
- Once an initial magnetic field discharge is established, very slowly increase the magnet current. Observe the anode voltage steadily rise; at the point where anode voltage begins to very rapidly increase, stop raising the magnetic field.
  - Adjust the propellant flow rate and/or anode current until the anode voltage very slightly drops or otherwise appears to stabilize.
  - If the thrust plume disappears, reduce the magnet current to 0A and then slowly raise it until the anode voltage nears where the plume disappeared.
- Repeat the process of incremental magnetic field raising until the maximum anode voltage or target magnetic field is reached:
  - The anode voltage increases to the target thruster value or power supply limit (e.g. 300 V for the authors)
  - The magnet current increases to the target thruster value.
  - Note that thruster could only achieve maximum anode voltage no higher than 23% of the designed magnet current.

Copyright 2024 by the Electric Rocket Propulsion Society. All rights reserved.

References

[1] Braden K Oh et al. "Undergraduate demonstration of a hall effect thruster: Self-directed learning in an advanced project context". In: *2020 ASEE Virtual Annual Conference Content Access*. 2020.

[2] Braden Oh et al. "Design, fabrication, and testing of an undergraduate hall effect thruster". In: *Journal of Electric Propulsion* 2.1 (2023), p. 6.

[3] James Wetherbee et al. "Student Design and Analysis of a Hall Effect Thruster". In: *AIAA SCITECH 2023 Forum*. 2023, p. 1598.

[4] Ishaan Mishra et al. "Development of an Undergraduate DC-Discharge Ring-Cusp Miniature Gridded Ion Thruster". In: *2024 IEEE Aerospace Conference*. IEEE. 2024, pp. 1–9.

[5] Ari J Eckhaus et al. "Student-led Design, Construction, and Testing of a Permanent Magnet Hall Thruster on Argon Propellant". In: *AIAA SCITECH 2024 Forum*. 2024, p. 1955.

[6] Leonard Cassady, Andrea Kodys, and Edgar Choueiri. "A thrust stand for high-power steady-state plasma thrusters". In: *38th AIAA/ASME/SAE/ASEE Joint Propulsion Conference & Exhibit*. 2002, p. 4118.

[7] Kurt A Polzin et al. "Thrust stand for electric propulsion performance evaluation". In: *Review of Scientific Instruments* 77.10 (2006).

[8] Harrison Adler et al. "Spectral Characterization of an Educational Hall Effect Thruster". 65th Annual APS DPP meeting, Denver, CO, Oct.30-Nov.3, 2023.

[9] YJ Hong et al. "Measurement of hydroxyl radical density generated from the atmospheric pressure bioplasma jet". In: *Journal of Instrumentation* 7.03 (2012), p. C03046.

[10] Meirong Dong et al. "Experimental study on the characteristics of molecular emission spectroscopy for the analysis of solid materials containing C and N". In: *Optics express* 19.18 (2011), pp. 17021–17029.

[11] Clabon Walter Allen. *Astrophysical quantities*. London: Athlone Press, 1973.

[12] Sidney Straus and Leo A Wall. "Pyrolysis of polyamides". In: *Journal of Research of the National Bureau of Standards* 60.1 (1958), p. 39.

[13] T Morikawa. "Formation of hydrogen cyanide by combustion and pyrolysis". In: *Bulletin of Japan Association for Fire Science and Engineering* 22.1_2 (1972), pp. 1–9.

[14] DP Stevenson. "Ionization and Dissociation by Electron Impact: Cyanogen, Hydrogen Cyanide, and Cyanogen Chloride and the Dissociation Energy of Cyanogen". In: *The Journal of Chemical Physics* 18.10 (1950), pp. 1347–1351.

[15] J Schutten et al. "Gross-and partial-ionization cross sections for electrons on water vapor in the energy range 0.1–20 keV". In: *The Journal of Chemical Physics* 44.10 (1966), pp. 3924–3928.

[16] James H Kyle and Glenn Hefter. "A critical review of the thermodynamics of hydrogen cyanide and copper (I)–cyanide complexes in aqueous solution". In: *Hydrometallurgy* 154 (2015), pp. 78–87.

[17] Dan M Goebel and Ira Katz. *Fundamentals of electric propulsion: ion and Hall thrusters*. Pasadena: NASA Jet Propulsion Laboratory, 2008.

[18] Marquardt, Niels. *Introduction to the principles of vacuum physics*. `http://dx.doi.org/10.5170/CERN-1999-005.1`. Accessed: July 1, 2023. 1999.

[19] Eunkwang Lee et al. "Scaling approach for sub-kilowatt Hall-effect thrusters". In: *Journal of Propulsion and Power* 35.6 (2019), pp. 1073–1079.

[20] Matthew Baird. "Designing an Accessible Hall Effect Thruster". In: *Honors Theses*. Kalamazoo, MI: Western Michigan University, 2016.

[21] Noah Zachary Warner. "Theoretical and experimental investigation of Hall thruster miniaturization". PhD thesis. Massachusetts Institute of Technology, 2007.

[22] Michael S McDonald and Alec D Gallimore. "Parametric Investigation of the Rotating Spoke Instability in Hall Thrusters". In: *International Electric Propulsion Conference*. IEPC-2011-242. 2011.

[23] Richard R Hofer et al. "Magnetic shielding of a laboratory Hall thruster. II. Experiments". In: *Journal of Applied Physics* 115.4 (2014).

Copyright 2024 by the Electric Rocket Propulsion Society. All rights reserved.